Spectral, spatial, and survivability evaluation of a flash-dried plasma-etched nanotube spray coating

MATTHEW T. SPIDELL,[1*] DAVIS R. CONKLIN,[1] CHRISTOPHER S. YUNG[1], EVANGELOS THEOCHAROUS [2], JOHN H. LEHMAN[1]

[1]National Institute of Standards and Technology, Boulder, Colorado 80305, USA
[2]National Physical Laboratory, Hampton Road, Teddington TW11 0LW, UK
*Corresponding author: Matthew.Spidell@NIST.GOV

Received XX Month XXXX; revised XX Month, XXXX; accepted XX Month XXXX; posted XX Month XXXX (Doc. ID XXXXX); published XX Month XXXX

We demonstrate improved manufacturability of spectrally flat detectors for visible to mid-infrared wavelengths by characterizing a carbon nanotube spray coating compatible with lithium tantalate and other thermal sensors. Compared against previous spray coatings, it demonstrated the highest responsivity yet attained due to both higher absorptivity and thermal diffusivity while also being matured to a commercially available product. It demonstrated spectral non-uniformity from 300 nm to 12 μm less than 1 % with uncertainty (k = 2) under 0.4 %. The spatial non-uniformity of the assembled sensor was less than 0.5 % over the central half (4 mm) of the absorber. As with previous developments employing isotropic carbon nanotube coatings, the absorber surface was sufficiently robust to withstand cleaning by compressed air-blast and survived repeated vacuum cycling without measurable impact upon responsivity.

OCIS codes: *(160.1890) Materials, Detector materials; (160.4236) Materials, Nanomaterials; (040.2235) Detectors, Far infrared or terahertz; (120.3150) Instrumentation, measurement, and metrology, Integrating spheres; 120.3940 Instrumentation, measurement, and metrology, Metrology.*

http://dx.doi.org/10.1364/AO.xx.xxxxxx

1. Introduction

Nanotube based absorbers combined with pyroelectric elements offer robust, spectrally flat, high responsivity thermo-optical detectors that achieve a higher signal-to-noise ratio than other room-temperature, broad-spectrum, radiometers [1, 2]. Previous work succeeded in depositing spectrally flat vertically aligned nanotube arrays (VANTAs) onto pyroelectric elements [3, 4] however, these proved difficult to manufacture and suffered reduced responsivity due to the manufacturing process and added thermal impedance. Previous nanotube-based spray coatings yielded higher responsivity than vertically aligned nanotube coatings but manifested spectral features in the near to mid-infrared [5, 1]. Gold black coatings, which demonstrated high responsivity and favorable spectral flatness in the VIS-NIR range, were susceptible to damage by irradiance exceeding 500 μW/mm^2 [6]. This contrasts with isotropic nanotube coatings that have been demonstrated to survive irradiance levels exceeding 1 W/mm^2 [7].

Lithium tantalate ($LiTaO_3$) was used as the pyroelectric crystal in this study. It was preferred over other pyroelectric materials because it is possible to produce large area crystals having uniform thickness and it offers a significantly higher figure of merit than comparable pyroelectric materials [8]. Unfortunately, the Curie temperature is below that of the chemical vapor deposition temperature for carbon nanotube growth [8] necessitating the use of sprayed nanotube coatings. Previous work indicates nonlinearity with this material class is under 0.2 % per decade [1]. Thinner crystals are preferred for their higher responsivity but suffer lower fabrication yield.

The theoretical underpinnings of carbon nanotube reflectivity and absorptivity have received much study, but without a unified theory yielding a complete description of their demonstrated low reflectivity over the VIS-THz wavelengths in close-packed structures. Comprehensive carbon nanotube review authors such as Saito et al. [9] Jorio et al. [10] and Harris et al. [11] in their respective works, use optical metrology of nanotubes in isolation to describe carbon nanotube metallic and semiconductor properties; however, these authors do not describe the bulk behavior of nanotube mats with their intrinsic geometry variation over a wide range of length scales (from under 10 nm to over 100 μm) which promotes light trapping capability not seen in isolation [12].

Several models have been put forward to describe the absorptivity of vertically aligned nanotube arrays [13] [14] in context of their complex electronic properties [15] [16] [17]. Isotropic nanotube structures do not follow the simplifying approximations used in these works (notably, uniform orientation and spacing). As such, nanotube coatings do not lend themselves to adequate analytical or numerical modeling. In general, the light trapping abilities are attributable to the complex electrical properties which, in closely packed nanotube

structures, produce bandgaps across a wide spectral range in conjunction with complex surface topology which significantly enhances structural absorption through multiple internal reflections [18, 19]. This necessitates empirical measurements of optical properties versus modeling.

Previous studies aimed at producing highly absorbing spectrally flat detector coatings [5, 7, 20] distinguish between single wall and multi-wall carbon nanotubes. However, these studies do not reveal significant differences in the optical properties of the nanotube coatings attributable to wall structure; both coatings lack spectral features departing from the 'continuum' reflection spectra. This lack of differentiation by spectral features may be explained by Garcia-Vidal et al., who suggest that while isolated hollow nanotubes can exhibit a well-defined dielectric function, in close packed structures, the presence of a hollow core becomes irrelevant due the presence of adjacent external structures which have a similar effect on the dielectric function as internal nanotube shells [13]. The continuum absorption appears to be dominated by large-scale surface topography and bond structure at nanotube termination [12, 21].

2. Device construction

The pyroelectric detector was fabricated from a 60 μm thick lithium tantalate crystal 12 mm in diameter which was the maximum aspect ratio we could practically handle. The crystal was coated with 20 nm nickel electrodes on each face. The nanotube mat absorber (detailed in section 3A) was deposited by overcoating the front electrode in an 8 mm circle as shown in Fig. 1. Silver bearing conductive epoxy bonded the front electrode to the case and an enameled wire filament was potted in conductive epoxy and bonded to the edge of the back electrode. The pyroelectric crystal was packaged in a 20 mm metal case. The case and front electrode function as a grounded shield to reduce the detectors sensitivity to electromagnetic interference.

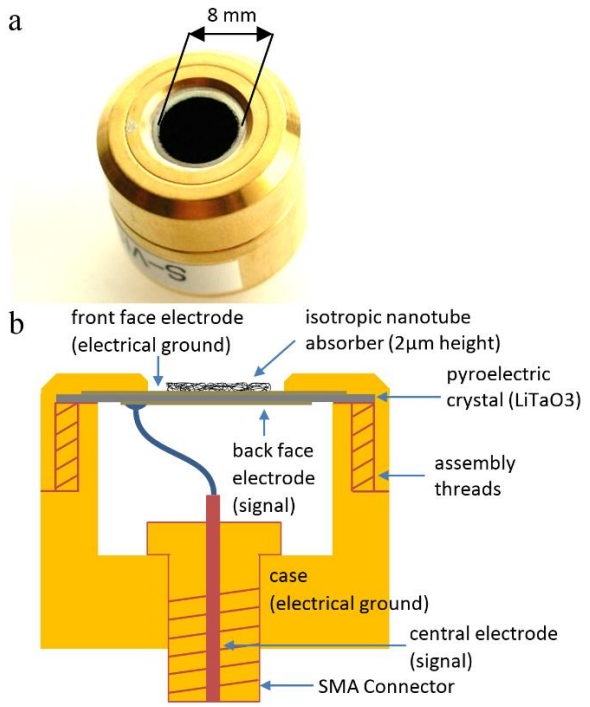

Fig. 1. Typical pyroelectric element with nanotube coating (a) Cross section of detector assembly (not to scale)

3. Coating Characteristics

Depicted in Fig. 2 at varying magnification, the coating is a carbon nanotube mat of isotropic non-directional fibers. The fibers form irregular cavities which, as with other percolated structures [5, 6], demonstrate effective light trapping capability approaching that of macroscopic cavities.

A. Coating constituents and deposition

The coating studied here is a proprietary (commercial) product and as such, the most specific details are withheld. The coating process is broadly outlined in its U.S. patent [22] and summarized here. Multi-wall nanotubes measuring 2 to 10 μm are suspended in a polar solvent or water with surfactants. The detector face is pre-heated to a temperature high enough to cause the solvent to flash dry when the suspension contacts it. Due to the pyroelectric effect, charge separation upon heating may cause dielectric breakdown of the crystal and low thermal ramp rates are required to prevent damage.

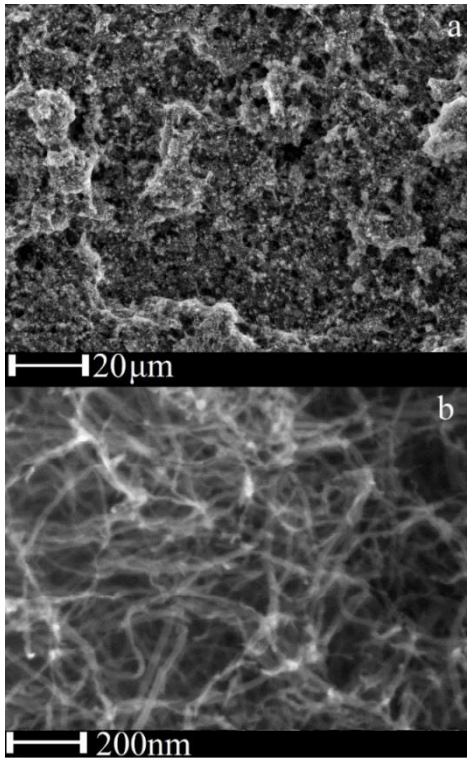

Fig. 2. Isotropic carbon nanotube coating (a) 20 μm scale (b) 200 nm scale

The nanotube suspension is deposited on the front electrode by a typical High Volume Low Pressure [23] spray system. The electrode is maintained at a temperature sufficient to promote solvent evaporation during coating application. The coating is applied in layers, until a film of carbon nanostructures at least 2 μm has been built-up. Finally, the nanotube coating is plasma etched to increase surface porosity. Further details of process variations including typical surface preparation, chemicals, and plasma energy densities are described in the patent [22] and not repeated here.

B. Spectral non-uniformity

Measurement results of the coating by the coating supplier [24] suggested reflectance under 0.5 % in the visible light regime, and below 0.2 % in the near infrared. Bidirectional reflectance distribution

function (BRDF) measurements conducted by a third party for the coating supplier indicate the coating approximates a Lambertian surface [25]. We undertook directional-hemispherical reflectance measurements of a witness sample from 0.3 µm to 16 µm and results are presented in Fig. **3**. A spectrophotometer was used for broadband measurements from 300 nm to 2500 nm while measurements from 1 µm to 15 µm were performed using a Fourier-transform infrared (FTIR) reflectometer. Both systems were commercial off-the-shelf hardware. For these broadband measurements, total hemispherical reflectance values were measured relative to NIST-traceable diffuse reflectance standards. Absolute reflectance measurements were performed using laser sources and a variation of Taylor's second absolute integrating sphere method [26]. These measurements at 405 nm, 657 nm, 1550 nm, and 10.6 µm provided tie points to appropriately scale the two broadband curves shown in Fig. 3. See Appendix A for further description of methods.

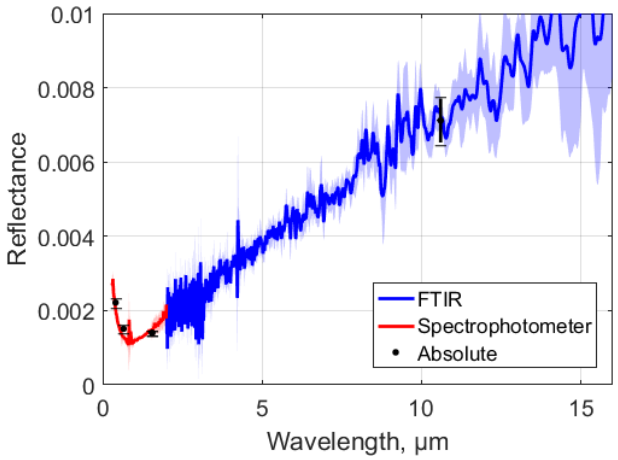

Fig. 3. Spectral reflectance of a carbon nanotube coating witness sample. Shaded areas surrounding the curves and error bars on the absolute reflectance measurements represent expanded uncertainty ($k = 2$).

Measured by precision spectrophotometers [27] at the United Kingdom's National Physical Laboratory (NPL) and plotted in Fig. 4, spectral responsivity of an assembled device demonstrated complimentary results to the above reflectance data. The relationship between spectral responsivity $S(\lambda)$ and spectral reflectance $R(\lambda)$ for an arbitrary irradiance $E(\lambda)$ may be expressed as $S(\lambda) = E(\lambda) * (1 - R(\lambda))$. With this relationship, as $R(\lambda) \rightarrow 0$ we find the slope $\Delta S/\Delta R \rightarrow 0$. As such, for low reflectance materials, the spectral responsivity shows negligible variation with wavelength given typical measurement uncertainties. In the present case, where the highest reflectance from 400 nm to 10 µm approaches 1 %, a standard uncertainty in the reflectance measurement of 20 % yields an expanded uncertainty ($k = 2$) of 0.4 %. Within the larger uncertainty bounds, the responsivity measurement agrees with the reflectivity measurements.

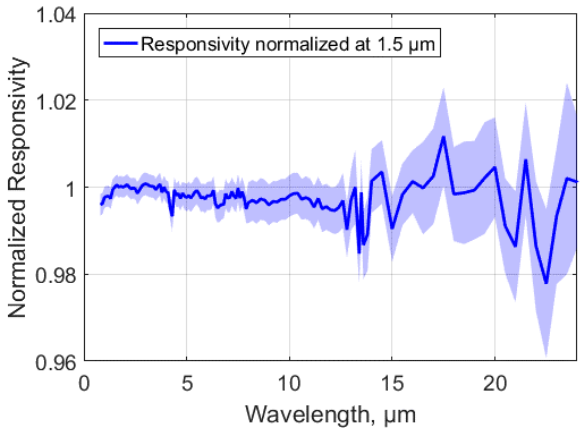

Fig. 4. Spectral responsivity of the assembled pyroelectric detector. This data was normalized to the response at 1.5 µm. The shaded region indicates expanded uncertainty ($k = 2$)

C. Vacuum compatibility

The survivability of the coating was established by cycling the material between atmospheric pressure and 200 mTorr, five times, with periods under vacuum and atmospheric pressure exceeding 12 hours for each cycle. Compared to a "control" device, the responsivity of the vacuum cycled device with a 632 nm, 1 mw, 1 mm diameter illuminating beam was unchanged. Microscopic inspection of the surface demonstrated no changes.

D. Spatial non-uniformity

The spatial non-uniformity of the coated pyroelectric detectors was assessed at NIST by raster scanning a 0.5 mm ($1/e^2$ diameter), 845 nm Gaussian laser beam providing a resolution of approximately 0.25 mm. Responsivity was normalized to the center. The results depicted in Fig. **6**, indicate the spatial non-uniformity over the central half of the 8 mm (diameter) coated area is under 0.5 %. Variations in responsivity may be attributed to variation in coating thickness or pyroelectric element thickness. When used in an overfilled condition for precision irradiance measurements, such spatial non-uniformity would present no effect on the responsivity, provided that the irradiance is uniform. However, should the irradiance underfill the active area, the spatial non-uniformity would introduce error. To estimate such error, we simulated a device calibrated with infinitesimal illuminated points located anywhere in the central half of the device. Given these assumptions, a Monte-Carlo simulation indicated the standard uncertainty contribution is approximately 0.2 %.

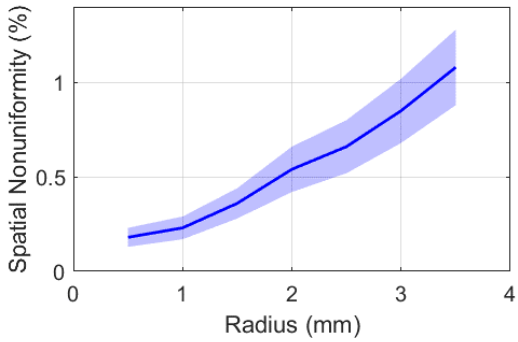

Fig. 5. Peak-to-trough spatial non-uniformity by radius from absorber center Shaded areas surrounding the curves and error bars on the absolute reflectance measurements represent expanded uncertainty ($k = 2$).

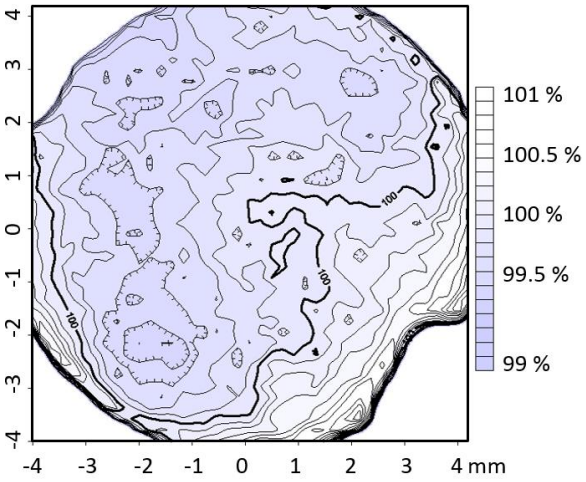

Fig. 6. Measured contour map of spatial non-uniformity.

4. Thermal diffusivity and pyroelectric sensitivity

Direct comparison of the frequency response of otherwise identically coated and uncoated pyroelectric elements under equivalent irradiance allows qualitative description of thin film thermal diffusivity. Precision measurement of the diffusivity is not practical due to the high relative uncertainty in the coating thickness. Normalized to an optical chopping frequency of 4 Hz, an uncoated pyroelectric crystal shows a responsivity decrease of 35 % from 4 Hz to 120 Hz while the coated pyroelectric shows a decrease of 43 %. For comparison, the first nanotube spray coatings [3] saw an 80 % reduction in responsivity. Due to its intrinsically low heat capacity and high thermal diffusivity, the first nanotube spray coating for radiometers developed by Lehman et al. [5] showed a responsivity at 632.8 nm of 0.339 μA/W (U = 0.86 %, k = 2) on a 60 μm thick lithium tantalate crystal while the coating in the present work shows a responsivity of 0.350 μA/W (U = 0.86 %, k = 2).

Measurements of frequency response were made by NPL and are described in Fig 7 below. The response is consistent with the trends demonstrated by similar previous devices [3, 4]. The optimum chopping frequency avoids the electrical supply line (60 Hz) harmonics and balances responsivity (improved by slower chopping rates) with reduction of microphonic noise contributions (improved by faster chopping frequencies).

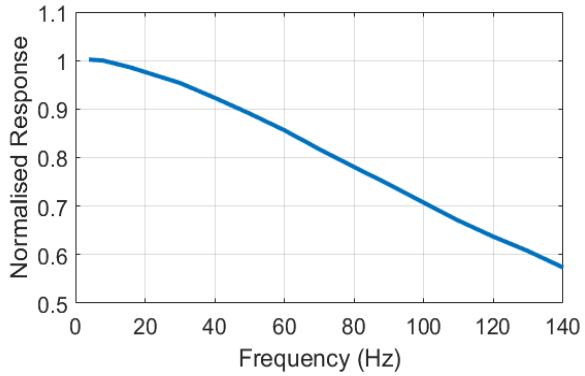

Fig 7. Normalized frequency response.

5. Discussion

The key technical improvements of this coating process over the methods outlined in previous work [1, 5] is the flash evaporation of solvent followed by plasma-etching to modify the surface topography to introduce greater porosity thereby increasing absorptivity, particularly in the infrared. As described in [21] plasma modification of nanotube surfaces introduces nanotube structural defects which cause absorption band broadening and increases 'macro' structure porosity which improves structural absorption by increasing the depth available for multiple-reflection absorption.

These devices offer, in effect, a spectrally flat reference detector and for applications as diverse as total solar irradiance monitoring and remote sensing system calibration. The spectral and spatial uniformity of this latest advancement in nanotube coatings suggest an avenue to produce reference grade spectrally flat sensors without extensive individual spectral characterization or overly conservative assumptions regarding spectral responsivity with correspondingly larger uncertainty. A single wavelength absolute calibration of a sensor offers accurate measurement over a wavelength span previously available only with detailed spectral responsivity scans.

Vacuum cycling suggests immunity to trapped gas damage mechanisms. With demonstrated robustness to air-blast and vacuum cycling, the coating warrants more aggressive thermal cycling, shock, and vibration testing to determine the extent of its reliability under adverse conditions ranging from handheld spectrometers to exo-atmospheric platforms.

Lower irradiance available for the spectral reflectivity and spectral responsivity measurements yielded increased uncertainty in the longwave infrared. While the data indicates spectral features could exist beyond 12 μm, they are limited to departures under 2 %, which still represents a significant improvement over previous coating technology [5]. The spectral flatness in the visible to mid-wave infrared approaches that of cavity absorbers [28, 29] and encourages use in planar bolometers. Both reflectance and absorptance measurements indicate spectral variation of less than 1 % at wavelengths from 300 nm to 12 μm.

6. Conclusions

We measured the spectral, spatial, and frequency response of a lithium tantalate pyroelectric detector with a commercially available carbon nanotube spray coating. The measurement results indicate that the coating does not compromise the detector responsivity and frequency response. The low reflectivity from 0.3 μm to 16 μm and spatial uniformity indicate the coating is suitable for production of reference-grade spectrally flat detectors. The process offers high commercial viability as a detector coating with few requirements beyond those of typical black paints. Compatibility of the coating with delicate pyroelectric elements suggests compatibility with other similarly delicate substrates, including MEMS devices or other similar devices with onboard electronic packages such as readout integrated circuits.

Appendix A

In this appendix, we detail the steps leading to the expression describing absolute reflectance as assessed by a variant on the Taylor absolute integrating sphere design [26]. The sphere design favored for this work features discreet (flanged) sample and reference ports, whereas the classic Taylor sphere employs a single knife edge port. While a single ideal (e.g. knife edged) sample port is preferred to eliminate higher order terms in the integrating sphere average reflectance expression [30], such a design can pose practical mechanical difficulties.

The Taylor sphere variant used in this research is illustrated in Fig. 8. Key details are the identical sample and reference ports, identical

entrance ports, and the baffle between the detector (or detectors field-of-view), and the sample. The utility of this design is demonstrated in the following expansions of the integrating sphere reflectance expression for sample and reference port illumination conditions. The ratio of these expressions yields Taylor's expression for directional-hemispherical reflectance of the sample material.

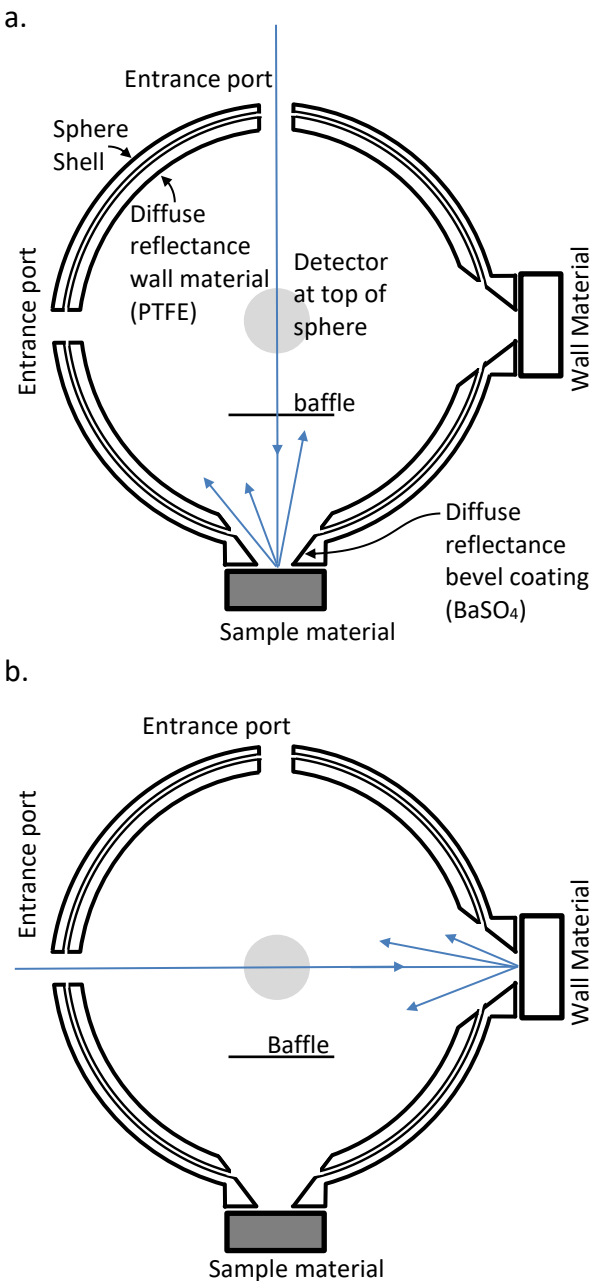

Fig. 8. Sketch of the integrating sphere used to perform absolute measurements of directional-hemispherical reflectance. (a) Configuration used when measuring V_s, and (b) is the configuration used when measuring V_r.

We used a variation of Taylor's second absolute method to measure the absolute reflectance values presented in Fig. 3. Only two measurements were needed to determine the absolute reflectance of a sample material using this method. The configurations required for these two measurements are shown in Fig. 8. In each configuration, the signal produced by a photodiode embedded in the top of the sphere is proportional to the radiant flux within the sphere [30]. This is attributed to the highly reflective and nearly Lambertian coating which covers the interior surface of the sphere. One method to approximate the flux within the sphere is to sum the flux that illuminates the sphere after each reflection. We assume that the sample and reference material are Lambertian, as carbon nanotubes have been shown to be very diffuse reflectors [31] and the reference material is the sphere wall coating.

Table 1. Nomenclature of integrating sphere equations

Term	Definition
A	Area
f	Exchange factor to sphere wall
V	Voltage signal measured by detector
ϕ	Initial radiant flux incident on the sample/reference material
ρ	Reflectance
$\bar{\rho}$	Average reflectance for a region of the sphere wall
Subscript	Definition
c	Sphere wall coating
d	Detector
en	Entrance port
ex	Exit port
r	Reference material
s	Sample
w	Entire sphere wall
$ws1$	Sphere wall illuminated by the first reflection from the sample
$wr1$	Sphere wall illuminated by the first reflection from the reference material

Symbols and subscripts applicable to the following derivation are outlined in Tab. 1. In the sample measurement configuration illustrated in Fig. 8(a), the sample is illuminated by flux ϕ_s and reflects $\phi_s\rho_s$ back into the sphere. The presence of a baffle between the sample and detector bars initially reflected light from being detected and it does not contribute to the signal V_s. Because we (safely) assume that the sample is Lambertian, the reflected light will then interact uniformly with the regions of the sphere which are visible to the sample. This is modeled using an area-weighted average reflectance $\bar{\rho}_{ws1}$. Because the baffle does not block any of these regions, this will contribute a flux of $\phi_s\rho_s\bar{\rho}_{ws1}$ which will be seen by the detector. After these first two reflections, we assume the effects of the baffle on the flux distribution within the sphere are negligible. As such, for each subsequent reflection we multiply by the area-weighted average reflectance of the entire integrating sphere $\bar{\rho}_w$ to determine the flux upon the detector. This yields a geometric series which may be simplified as follows:

$$V_s \propto \phi_s\rho_s\bar{\rho}_{ws1} + \phi_s\rho_s\bar{\rho}_{ws1}\bar{\rho}_w + \phi_s\rho_s\bar{\rho}_{ws1}\bar{\rho}_w^2 + \ldots + \phi_s\rho_s\bar{\rho}_{ws1}\bar{\rho}_w^n$$

$$V_s \propto \phi_s\rho_s\bar{\rho}_{ws1}\sum_{n=0}^{\infty}\bar{\rho}_w{}^n$$

$$V_s \propto \frac{\phi_s\rho_s\bar{\rho}_{ws1}}{1-\bar{\rho}_w} \quad (1)$$

Note that a proportionality symbol is used as we neglect to include the instrument factor (i.e. power to signal constant). This factor is invariant during measurement and divides out of the latter results along with the incident flux term ϕ.

As with the above, we approximate the total flux within the sphere during measurement in the reference configuration described by Fig. 8(b). The key difference is the absence of a baffle between the reference material and detector, which allows the flux from the first reflection off

the material $\phi_r\rho_r$ to yield a signal from the detector. The first reflection from the reference material will also encounter different regions of the sphere than the first reflection from the sample, so the area-weighted average reflectance of this region $\bar{\rho}_{wr1}$ is used in place of $\bar{\rho}_{ws1}$. A different input flux ϕ_r is also specified to account for source instability.

$$V_r \propto \phi_r\rho_r + \phi_r\rho_r\bar{\rho}_{wr1} + \phi_r\rho_r\bar{\rho}_{wr1}\bar{\rho}_w + \phi_r\rho_r\bar{\rho}_{wr1}\bar{\rho}_w^2 + \phi_r\rho_r\bar{\rho}_{wr1}\bar{\rho}_w^n$$

$$V_r \propto \phi_r\rho_r + \phi_r\rho_r\bar{\rho}_{wr1}\sum_{n=0}^{\infty}\bar{\rho}_w{}^n$$

$$V_r \propto \phi_r\rho_r + \frac{\phi_r\rho_r\bar{\rho}_{wr1}}{1-\bar{\rho}_w} \quad (2)$$

To isolate the sample reflectance, we ratio equations (1) and (2). Using the same detector and associated electronics, the proportionality constants will cancel leaving the following:

$$\frac{V_s}{V_r} = \frac{\phi_s\rho_s\bar{\rho}_{ws1}/(1-\bar{\rho}_w)}{\phi_r\rho_r + \phi_r\rho_r\bar{\rho}_{wr1}/(1-\bar{\rho}_w)}$$

$$\frac{V_s}{V_r} = \frac{\phi_s\rho_s\bar{\rho}_{ws1}}{\phi_r\rho_r(1-\bar{\rho}_w+\bar{\rho}_{wr1})} \quad (3)$$

$$\rho_s = \frac{V_s}{V_r}\left[\frac{\phi_r\rho_r(1-\bar{\rho}_w+\bar{\rho}_{wr1})}{\phi_s\bar{\rho}_{ws1}}\right] \quad (4)$$

We describe the area-averaged reflectance terms by introducing exchange factors f_i for each port i, which for a sphere is simply given by the ratio of the port area to the sphere area, A_i/A_w:

$$\bar{\rho}_w = \rho_c(1-2f_{en}-2f_{ex}-f_d) + f_{ex}\rho_r + f_{ex}\rho_s + f_d\rho_d \quad (5)$$

$$\bar{\rho}_{ws1} = \rho_c(1-2f_{en}-f_{ex}) + f_{ex}\rho_r \quad (6)$$

$$\bar{\rho}_{wr1} = \rho_c(1-2f_{en}-f_{ex}-f_d) + f_{ex}\rho_s + f_d\rho_d \quad (7)$$

Upon substituting these expressions into equation (3), we are left with the following expression for sample reflectance:

$$\rho_s = \frac{V_s}{V_r}\left[\frac{\phi_r\rho_r\big(1+f_{ex}(\rho_c-\rho_r)\big)}{\phi_s(\rho_c(1-2f_{en}-f_{ex})+f_{ex}\rho_r)}\right] \quad (8)$$

We now apply the assumption of identical reflectance of the reference material and sphere wall coating $\rho_r = \rho_c$. We also assume that the incident flux during the sample and reference measurements is identical, which is assured in practice by performing repeated measurements and/or beam stabilization while alternating between configurations described in Fig. 8. Applying these simplifications yields the final expression,

$$\rho_s = \frac{V_s}{V_r}\left[\frac{1}{1-2f_{en}}\right] \quad (9)$$

matching Taylor's second absolute method [26], despite the differing configuration of our integrating sphere.

REFERENCES

1. E. Theocharous and J. Lehman, "The evaluation of a pyroelectric detector with and without a sprayed multi-walled carbon nanotube coating," Infrared Phy. and Technol. **55**, 161-165 (2012).
2. E. Dereniak and G. Boreman, *Infrared Detectors and Systems* (Wiley, 1996).
3. J. H. Lehman, E. Theocharous and S. Theocharous, "Assembly and evaluation of a pyroelectric detector bonded to vertically aligned multiwalled carbon nanotubes over thin silicon," App. Opt. **52**, 8054-8059 2013.
4. J. H. Lehman, A. W. Sanders, L. M. Hanssen, B. Wilthan, J. Zeng and C. Jensen, "Very black infrared detector from vertically aligned carbon nanotubes and electric-field poling of lithium tantalate," Nano Lett. **10**, 3261-3266 2010.
5. J. Lehman, C. Engtrakul, T. Gennett and A. Dillon, "Single Wall Carbon Nanotube Coating on a Pyroelectric Detector," App. Opt. **44**, 483-488 2005.
6. J. Lehman, E. Theocharous, G. Eppeldauer and C. Pannell, "Gold-black coatings for freestanding pyroelectric detectors," Measurement Science and Technology **14**, 916–922 2003.
7. K. Ramadurai, C. L. Cromer, L. A. Lewis, K. E. Hurst, A. C. Dillon, R. L. Mahajan and J. H. Lehman, "High-performance carbon nanotube coatings for high-power laser radiometry," J. App. Phys. **103**, 013103-1 2008.
8. T. Yokoo, K. Shibata and Y. Kuwano, "Application of Pyroelectricity of LiTaO3 for Infrared Detectors," Japanese Journal of Applied Physics **24**, 149-152 1985.
9. R. Saito, M. Dresselhaus and G. Dresselhaus, *Physical Properties of Carbon Nanotubes* (Imperial College Press, 1998).
10. A. Jorio, M. S. Dresselhaus and G. Dresselhaus, *Carbon Nanotubes* (Springer, 2008).
11. P. J. F. Harris, *Carbon Nanotubes and Related Structures* (Cambridge University Press, 1999).
12. J. H. Lehman, C. S. Yung, D. R. Conklin, N. A. Tomlin and M. S. Stephens, "Carbon nanotube-based black coatings," App. Phys. Rev. **5**, 011103 2018.
13. F. J. Garcia-Vidal, J. M. Pitarke and J. B. Pendry, "Effective Medium Theory of the Optical Properties of Aligned Carbon Nanotubes," Phys. Rev. Lett., **78**, 4289-4292 1997.
14. F. Wang, G. Dukovic, L. E. Brus and T. F. Heinz, "The Optical Resonances in Carbon Nanotubes Arise from Excitons," Science, **308** 838-841 2005.
15. M. Bockrath, D. H. Cobden, L. McEuen, N. G. Chopra, A. Zettl, A. Thess and R. E. Smalley, "Single-Electron Transport in Ropes of Carbon Nanotubes," Science **275**, 1922-1925 1997.
16. T. W. Odom1, J.-L. Huang, C. L. Cheung and C. M. Lieber, "Magnetic Clusters on Single-Walled Carbon Nanotubes: The Kondo Effect in a One-Dimensional Host," Science **290**, 1549-1552 2000.
17. M. Bockrath, D. H. Cobden, J. Lu, A. G. Rinzler, R. E. Smalley, L. Balents and L. McEuen, "Luttinger-liquid behaviour in carbon nanotubes," Nature **397**, 598–601 1999.
18. A. Y. Vorobyev and C. Guoa, "Colorizing metals with femtosecond laser pulses," App. Phys. **92**, 041914 2008.
19. J. L. Haiyan Tao, Z. Hao, X. Gao, X. Song, C. Sun and X. Tan, "Formation of strong light-trapping nano and microscale structures on a spherical metal surface by femtosecond laser filament," App. Phys. Lett. **100**, 201111 2012.
20. T. W. Ebbesen, *Carbon Nanotubes: Preparation and Properties* (CRC Press, 1997).
21. C. S. Yung, N. A. Tomlin, K. Heuerman, M. W. Keller, M. G. White, M. S. Stephens and J. H. Lehman, "Plasma modification of vertically aligned carbon nanotubes: superhydrophobic surfaces with ultra- low reflectance," ACS Nano Lett. **127**, 195-201 2018.
22. N. W. March, "Low Reflectivity Coating and Method And System for Coating a Substrate," U.S. Patent 20180201541 (2016).
23. W. A. Heitbrink, R. H. Verb, T. J. Fischbach and M. A. Wallace, "A Comparison of Conventional and High Volume-Low Pressure Spray-Painting Guns," American Industrial Hygiene Association Journal **57**, 304-310 1996.
24. "S-VIS Ultra Black Spray-Applied Coating Technical Data Sheet. Surrey Nanosystems, London, U.K." 2017, https://www.surreynanosystems.com/assets/media/vantablack-vb-a4-data-brochure-2016-009-download.pdf. Accessed 31 August 2017
25. "S-VIS BRDF data. Surrey Nanosystems, London, U.K." 2017, https://www.surreynanosystems.com/assets/media/vantablack-s-vis-a4-data-brochure-2017-026.pdf. Accessed 31 August 2018

26. A. H. Taylor, "The Measurement of Diffuse Reflection Factors and a New Absolute Reflectometer," J. OSA **4**, 9-23 1920.
27. E. Theocharous, F. Clarke, L. Rodgers and N. Fox, "Latest techniques at NPL for the characterisation of infrared detectors and materials," Proc. SPIE **5209**, 228-239 (2003).
28. O. Touayar, B. Rougie, J. M. Coutin and J. Bastie, "Measurement of the reactance of the INM cryogenic radiometer cavity at several wavelengths," Metrologia **35**, 387-391 (1998).
29. J. C. Molina, J. J. S. Bernal, H. A. Castillo and M. R. Gonzalez, "Electrical substitution radiometer cavity absorptance measurement," J. Int. Meas. Confed. **64**, 89-93 (2015).
30. L. M. Hanssen and K. A. Snail, "Integrating Spheres for Mid- and Near-infrared Reflection Spectroscopy," in *Handbook of Vibrational Spectroscopy,* (Wiley, 2002), pp. 1-18
31. C. L. Cromer, K. Hurst, X. Li and J. Lehman, "Black optical coating for high-power laser measurements from carbon nanotubes and silicate," Opt. Lett. **34**, 193-195 2009.

References

1. E. Theocharous and J. Lehman, "The evaluation of a pyroelectric detector with and without a sprayed multi-walled carbon nanotube coating," Infrared Phy. and Technol. **55**, 161-165 (2012).
2. E. Dereniak and G. Boreman, *Infrared Detectors and Systems* (Wiley, 1996).
3. J. H. Lehman, E. Theocharous and S. Theocharous, "Assembly and evaluation of a pyroelectric detector bonded to vertically aligned multiwalled carbon nanotubes over thin silicon," App. Opt. **52**, 8054-8059 2013.
4. J. H. Lehman, A. W. Sanders, L. M. Hanssen, B. Wilthan, J. Zeng and C. Jensen, "Very black infrared detector from vertically aligned carbon nanotubes and electric-field poling of lithium tantalate," Nano Lett. **10**, 3261-3266 2010.
5. J. Lehman, C. Engtrakul, T. Gennett and A. Dillon, "Single Wall Carbon Nanotube Coating on a Pyroelectric Detector," App. Opt. **44**, 483-488 2005.
6. J. Lehman, E. Theocharous, G. Eppeldauer and C. Pannell, "Gold-black coatings for freestanding pyroelectric detectors," Measurement Science and Technology **14**, 916–922 2003.
7. K. Ramadurai, C. L. Cromer, L. A. Lewis, K. E. Hurst, A. C. Dillon, R. L. Mahajan and J. H. Lehman, "High-performance carbon nanotube coatings for high-power laser radiometry," J. App. Phys. **103**, 013103-1 2008.
8. T. Yokoo, K. Shibata and Y. Kuwano, "Application of Pyroelectricity of LiTaO3 for Infrared Detectors," Japanese Journal of Applied Physics **24**, 149-152 1985.
9. R. Saito, M. Dresselhaus and G. Dresselhaus, *Physical Properties of Carbon Nanotubes* (Imperial College Press, 1998).
10. A. Jorio, M. S. Dresselhaus and G. Dresselhaus, *Carbon Nanotubes* (Springer, 2008).
11. P. J. F. Harris, *Carbon Nanotubes and Related Structures* (Cambridge University Press, 1999).
12. J. H. Lehman, C. S. Yung, D. R. Conklin, N. A. Tomlin and M. S. Stephens, "Carbon nanotube-based black coatings," App. Phys. Rev. **5**, 011103 2018.
13. F. J. Garcia-Vidal, J. M. Pitarke and J. B. Pendry, "Effective Medium Theory of the Optical Properties of Aligned Carbon Nanotubes," Phys. Rev. Lett., **78**, 4289-4292 1997.
14. F. Wang, G. Dukovic, L. E. Brus and T. F. Heinz, "The Optical Resonances in Carbon Nanotubes Arise from Excitons," Science, **308** 838-841 2005.
15. M. Bockrath, D. H. Cobden, L. McEuen, N. G. Chopra, A. Zettl, A. Thess and R. E. Smalley, "Single-Electron Transport in Ropes of Carbon Nanotubes," Science **275**, 1922-1925 1997.
16. T. W. Odom1, J.-L. Huang, C. L. Cheung and C. M. Lieber, "Magnetic Clusters on Single-Walled Carbon Nanotubes: The Kondo Effect in a One-Dimensional Host," Science **290**, 1549-1552 2000.
17. M. Bockrath, D. H. Cobden, J. Lu, A. G. Rinzler, R. E. Smalley, L. Balents and L. McEuen, "Luttinger-liquid behaviour in carbon nanotubes," Nature **397**, 598–601 1999.
18. A. Y. Vorobyev and C. Guoa, "Colorizing metals with femtosecond laser pulses," App. Phys. **92**, 041914 2008.
19. J. L. Haiyan Tao, Z. Hao, X. Gao, X. Song, C. Sun and X. Tan, "Formation of strong light-trapping nano and microscale structures on a spherical metal surface by femtosecond laser filament," App. Phys. Lett. **100**, 201111 2012.
20. T. W. Ebbesen, C*arbon Nanotubes: Preparation and Properties* (CRC Press, 1997).
21. C. S. Yung, N. A. Tomlin, K. Heuerman, M. W. Keller, M. G. White, M. S. Stephens and J. H. Lehman, "Plasma modification of vertically aligned carbon nanotubes: superhydrophobic surfaces with ultra- low reflectance," ACS Nano Lett. **127**, 195-201 2018.
22. N. W. March, "Low Reflectivity Coating and Method And System for Coating a Substrate," U.S. Patent 20180201541 (2016).
23. W. A. Heitbrink, R. H. Verb, T. J. Fischbach and M. A. Wallace, "A Comparison of Conventional and High Volume-Low Pressure Spray-Painting Guns," American Industrial Hygiene Association Journal **57**, 304-310 1996.
24. "S-VIS Ultra Black Spray-Applied Coating Technical Data Sheet. Surrey Nanosystems, London, U.K." 2017, https://www.surreynanosystems.com/assets/media/vantablack-vb-a4-data-brochure-2016-009-download.pdf. Accessed 31 August 2017
25. "S-VIS BRDF data. Surrey Nanosystems, London, U.K." 2017, https://www.surreynanosystems.com/assets/media/vantablack-s-vis-a4-data-brochure-2017-026.pdf. Accessed 31 August 2018
26. A. H. Taylor, "The Measurement of Diffuse Reflection Factors and a New Absolute Reflectometer," J. OSA **4**, 9-23 1920.
27. E. Theocharous, F. Clarke, L. Rodgers and N. Fox, "Latest techniques at NPL for the characterisation of infrared detectors and materials," Proc. SPIE **5209**, 228-239 (2003).
28. O. Touayar, B. Rougie, J. M. Coutin and J. Bastie, "Measurement of the reactance of the INM cryogenic radiometer cavity at several wavelengths," Metrologia **35**, 387-391 (1998).
29. J. C. Molina, J. J. S. Bernal, H. A. Castillo and M. R. Gonzalez, "Electrical substitution radiometer cavity absorptance measurement," J. Int. Meas. Confed. **64**, 89-93 (2015).
30. L. M. Hanssen and K. A. Snail, "Integrating Spheres for Mid- and Near-infrared Reflection Spectroscopy," in *Handbook of Vibrational Spectroscopy,* (Wiley, 2002), pp. 1-18
31. C. L. Cromer, K. Hurst, X. Li and J. Lehman, "Black optical coating for high-power laser measurements from carbon nanotubes and silicate," Opt. Lett. **34**, 193-195 2009.